http://dx.doi.org/10.5772/intechopen.69792

2.3.4. Contour-based segmentation technique

The contour-based segmentation algorithm works in five steps as follows:

Step 1: Read the preprocessed image as input image.

Step 2: By performing the morphological operations, the abnormality is super imposed on original image.

Step 3: Apply active contour technique to identify the suspicious lesions; the suspicious lesions are peaks of the contour.

Step 4: Extract peak of the contour by calculating the energy of each contour.

Step 5: Mark extracted contour as ROI.

The stepwise results are shown in **Figure 14**. Energy of the contour is calculated by adding the intensity of pixels from each contour and finding average. Average of each contour is compared to select the mass region.

The contour-based technique works well on all kinds of tissues like fatty, glandular, and dense as shown in **Figure 15**. Also it works with high-intensity and low-intensity images.

2.4. Feature extraction of mass ROI

Radiologists depict masses by their shape, gray levels, and texture properties. The properties of mass surroundings are important discriminators from the background tissue. The shape of the mass changing from early benign to malignant as round, oval, lobular, or irregular circumscribed, micro-lobulated, obscured, indistinct, or peculated [36–39]. **Figure 16** shows a schematic diagram of mass shapes and boundary characteristics differ from benign to malignant. We also note that masses with speculated and indistinct boundaries have a greater probability of malignancy than circumscribed masses.

It also notes that masses with speculated and indistinct boundaries have a greater probability of malignancy than circumscribed masses. Along with the mass margin and shape, intensity of gray level is one of major feature to classify the mass. Hence, in this CAD system, different

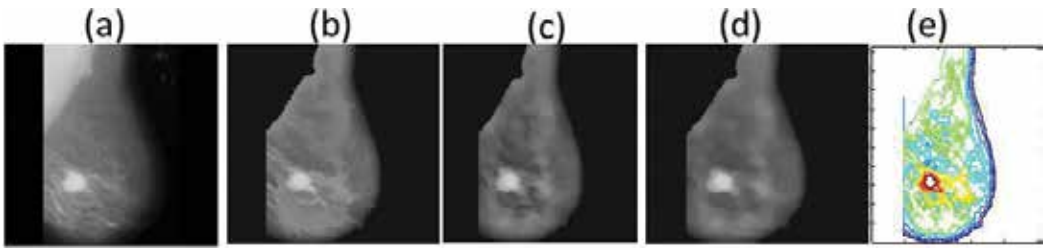

Figure 14. Experimental results of contour-based segmentation technique (a) original image, (b) preprocessed image, (c) opening, (d) closing, (e) reconstructed from opening and closing, (f) active contour.

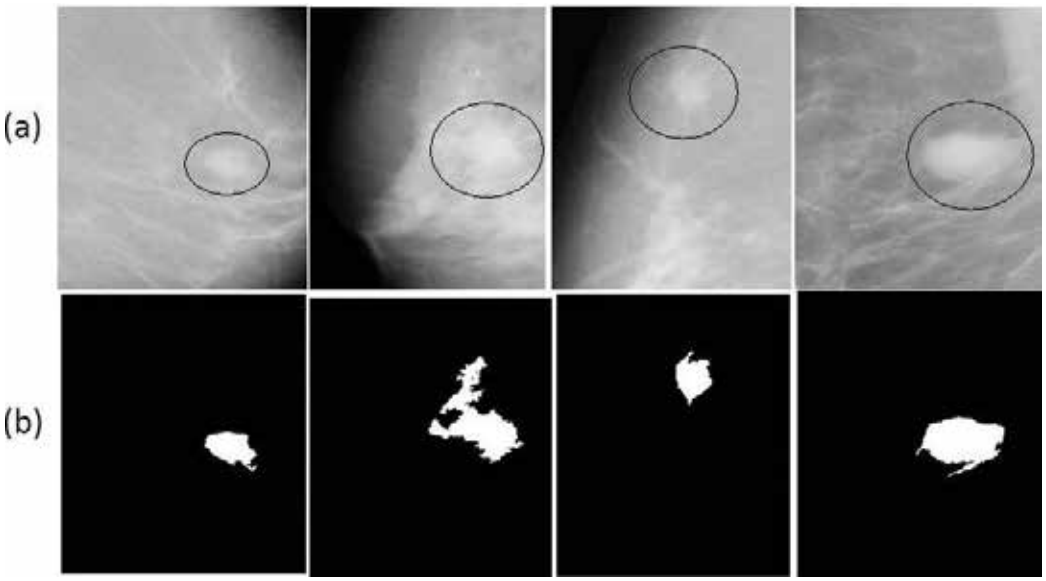

Figure 15. Mass segmented on different tissues using contour-based segmentation. (a) Ground truth (b) results of proposed work.

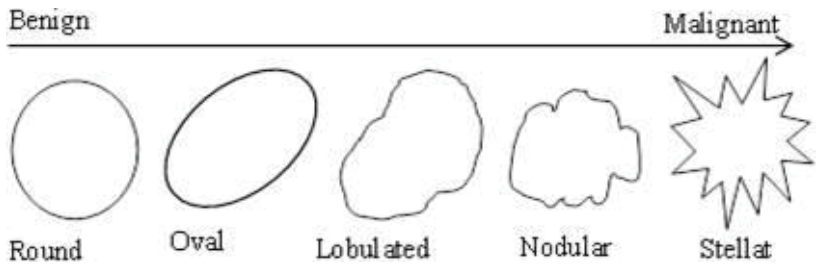

Figure 16. Morphological changes of mass in image from benign to malignant.

features have extracted by wavelet features, Gray Level Co-Occurrence Matrix (GLCM) features, and Segmentation-based Fractal Texture Analysis (SFTA) features calculated.

2.4.1. Discrete wavelet transform (DWT)

The DWT is wavelet transform using discrete set of scales and translations followed by some rules. To use a wavelet, it is necessary to discretize with respective to scale parameters, i.e., sampling. The scale and translation parameters are given by, $S = 2 -$ m and $T = n2 - m$, where m and n are the subset of all integers. Thus, the family of wavelet is defined in Eq. (6).

$$\psi_{m,n} = 2^{\frac{m}{2}}\psi(2^m t - n) \tag{6}$$

http://dx.doi.org/10.5772/intechopen.69792

The wavelet transform decomposes a signal $\chi(t)$ into a family of wavelets as given in Eq. (7).

$$\chi(t) = \sum_m \sum_n c_{m,n} \psi_{m,n}(t) \tag{7}$$

where

$$C_{m,n} = \{x(t), \psi_{m,n}(t)$$

For a discrete time signal $x[n]$, the decomposition is given by Eq. (8):

$$x[n] = \sum_{i=1 \text{ to } l} \sum_{k \epsilon Z} C_{i,k} g[n - 2^i k] + \sum_{k \epsilon Z} d_{1,k} h_1[n - 2^i k] \tag{8}$$

In case of images, the DWT is applied to each dimensionality, separately. The resulting image X is decomposed in first level is xA, xH,xV, and xD as approximation, horizontal, vertical, and diagonal, respectively. The xA component contains low frequency components and remaining contains high frequency component. Hence, X= xA + {xH + xV + xD}. Then, DWT applied to xA for second level decomposition. Hence, the wavelet provides hierarchical framework to interpret the image information [40, 41]. The basis of wavelet transform is localized on mother wavelet. Hence, in the proposed work, Haar, Daubechies (db2,db4 and db8), coiflet and bi-orthogonal wavelets at decomposition of level 4 used for the dataset and passed feature vector for the classification.

2.4.2. GLCM features

In texture analysis, widely used features are GLCM features. The GLCM is representation of frequently occurred gray levels combinations [42]. It is second order statistics that can be used to analyzing the texture features based on number of pixels in different combinations as shown in **Figure 17**. The matrices are constructed at different gray levels, such as 1, 2, 3, 4, and so on, for the different directions, such as 0, 45, 90, 180° and so on. Depends on the number of combinations the statistics are measured as features in first order, second order, and in higher

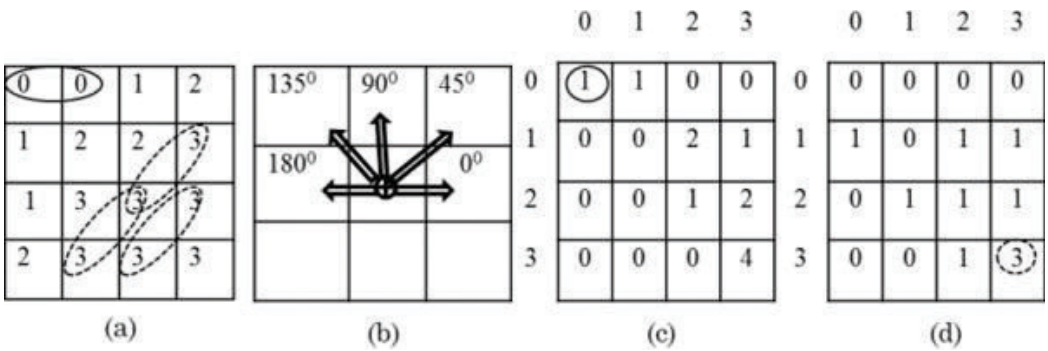

Figure 17. Example of GLCM (a) four-level gray image, (b) direction of combination with single pixel distance, (c) covariance matrix of four levels with direction 00 with single pixel distance, and (d) co-variance matrix of four levels with direction 450 with single pixel distance.

orders. Initially Haralick et al. [43] has defined 13 GLCM features then Soh and Tsatsoulis [44], and Clausi [45] have increased them to 21 features. In most of the CAD systems, these gray level features are used to interpret the symptoms. In the proposed work, we have extracted 21 GLCM features which are contributing to the discrimination of mass type.

2.4.3. SFTA features

Texture feature extraction is time-consuming process with basic filters because of scale and time invariant. This time consuming problem overcome by applying SFTA algorithm proposed by Costa [46]. SFTA works on multilevel thresholding on gray image. In purpose of using SFTA is to get the clear structure for mass boundaries. The 21 texture feature vector corresponds to texture information like dimension, different gray levels, and area of ROI. The region-based 21 shape features extracted from the ROI such as area, orientation, bounding box, extent, perimeter, centroid, extrema, pixel_idx_list, convex area, filled area, pixel list, convex hull, filled image, solidity, convex image, sub_array_idx, eccentricity, major_axis_length, equi_diameter, minor_axis_length, and Euler number. All together there are 73 features extracted from mass to train the CAD system to discriminate the mass type as benign and malignant [48].

2.5. Classification

Support vector machine (SVM) is a supervised learning technique that seeks an optimal hyperplane to separate two classes of samples. Mapping the input data into a higher dimensional space is done by using Kernel functions with the aim of obtaining a better distribution of the data. Then, an optimal separating hyperplane in the high-dimensional feature space can be easily found as shown in Ref. [47]. An example of an optimal hyperplane is shown in **Figure 18**.

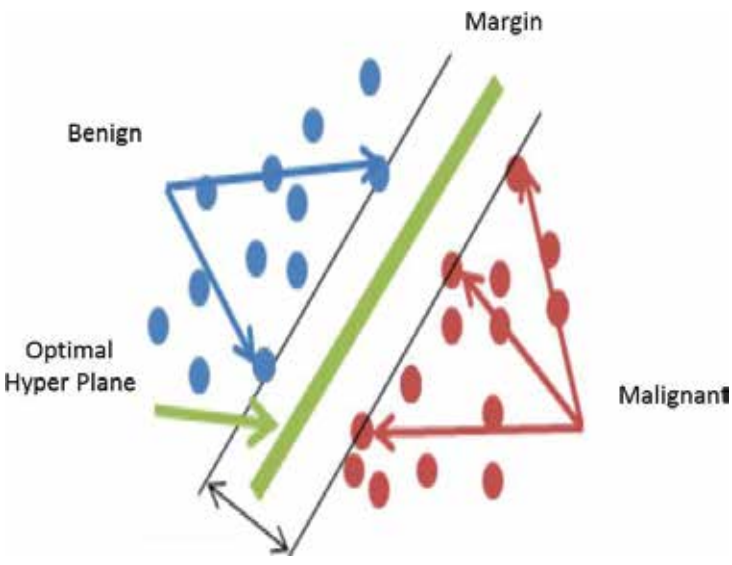

Figure 18. Optimum hyperplane for support vector machine.

3. Experimental results

The proposed algorithm implemented in MATLAB13a, classification accuracy measured with confusion matrix shown in **Table 1** and tested on MIAS dataset. MIAS contains a total of 322 mammograms of both breasts (left and right) of 161 patients.

According to above definitions of true positive, true negative, false positive and false negative. The equations related to specificity (the accuracy of negative class), sensitivity (accuracy of positive class and accuracy), and accuracy of recognize both negative and positive classes are defined as in Eqs. (9)–(11), respectively.

$$\text{Specificity} = \left(\frac{\text{TN}}{\text{TN} + \text{FP}}\right) * 100 \tag{9}$$

$$\text{Sensitivity} = \left(\frac{\text{TP}}{\text{TP} + \text{FN}}\right) * 100 \tag{10}$$

$$\text{Accuracy} = \left(\frac{\text{TP} + \text{TN}}{\text{TP} + \text{TN} + \text{FP} + \text{FN}}\right) * 100 \tag{11}$$

Classification measured based on different feature extraction techniques with contour-based segmentation and SVM classifier as shown in **Table 2**, the number of images used to test the system is 50, and among them, 37 are malignant cases and 13 are benign cases. The accuracy is high using wavelet db4 features [50].

Though wavelet db4 gives high accuracy, it is important to consider texture based and gray level features to discriminate the mass type as benign and malignant. Hence, for the proposed CAD model all features together passed to measure the performance of algorithm with different segmentation techniques such as adaptive threshold-based technique, modified segmentation technique, and energy-based contour segmentation shown in **Table 3**.

Actual/predicted classes	Benign	Malignant
Benign	TP	FP
Malignant	FN	TN

Table 1. Confusion matrix.

Parameters	GLCM	Wavelet dB4	SFTA	Stats from region props
Total number of images	50	50	50	50
Number of benign images	13	13	13	13
Number of malignant Images	37	37	37	37
Number of misclassification	04	02	03	05
Accuracy (%)	92	96	94	90

Table 2. Samples used for performance evaluation.

Segmentation techniques	Accuracy	Specificity	Sensitivity
Adaptive threshold based	97.32143	98.03922	96.72131
Modified watershed segmentation	96.46018	100	93.75
Energy-based contour segmentation	98.26087	100	96.8254

Table 3. The performance measures of the SVM classifier with different similarity matrices.

Comparing with all the three techniques, energy-based technique gives more accurate results as shown in **Figure 19**.

The performance of the classifier compared with previous work shown in **Table 4**, the combination of different features achieved more accuracy comparing with existing work.

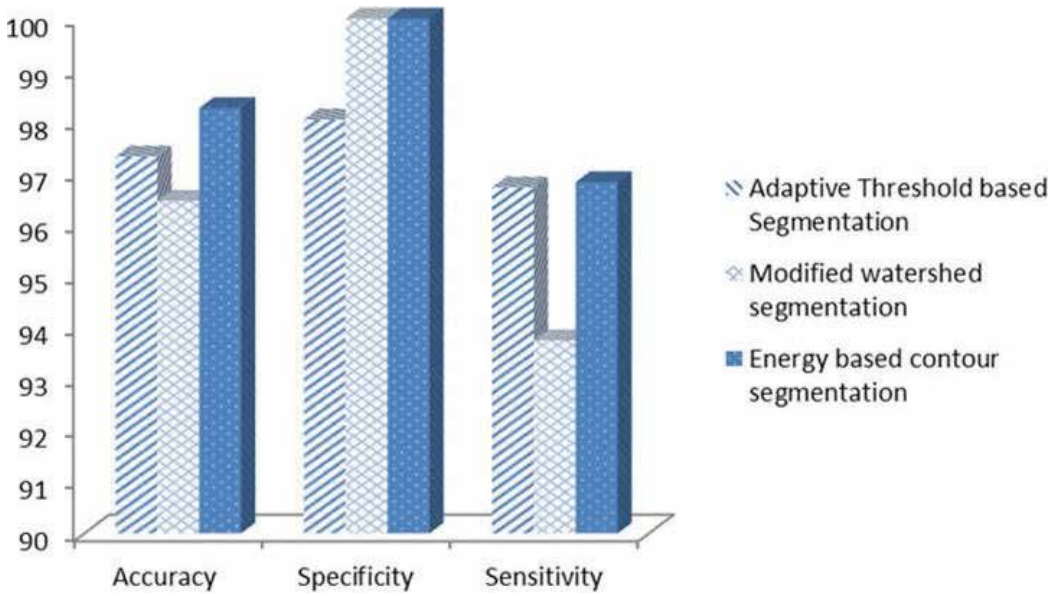

Figure 19. Comparative analysis of accuracy rate for adaptive threshold, modified watershed, and energy-based contour segmentation techniques.

Features	Classifier	Accuracy (%)	Reference
Fractal features	SVM	85.7	S. D. Tzikopoulos et al. (2011) [48]
SIFT, LBP, texton histogram	SVM	93.54	G. Liasis et al. (2011) [49]
GLCM, statistical, histogram (ROI)	K-NN	82.5	M. Mario et al. (2012) [50]
Statistical moments (ROI)	Combined K-NN	91.72	K. Vaidehi and T. S. Subashini (2015)[51]
Db4 wavelet, GLCM, SFTA features	SVM	98.26	Proposed method

Table 4. Comparison of preset algorithm with previous works reported.

http://dx.doi.org/10.5772/intechopen.69792

4. Discussion

Early detection of breast cancer may reduce the death rate. The advancement in technology is needed in the detection of all types of masses in terms of increasing sensitivity and reducing false positive rate. Masses can be varying in size and shape and thus, the proposed segmentation and feature extraction techniques are more suitable to measure in terms. As the experimental results reported based on individual feature sets such as GLCM, wavelet, SFTA, and region-based statistical features, the accuracy was 92, 96, 94, and 90%, respectively as observed in **Table 2**. With same segmentation technique accuracy is increased by passing combined set of features to SVM classifier as shown in **Table 3**. The CAD system is compared with different set of features with different classifiers as shown in **Table 4**. It proved that with less number of features and simple classifier, it improved the accuracy of detection and classification with less complexity.

5. Conclusion

The CAD system is used to help the radiologists to interpret the medical images like mammography, X-ray, ultrasound, MRI, etc. It used as a second opinion by the radiologists. Improving CAD accuracy increases the treatment option and a cure is more likely. There are some commercial CAD systems that have been reported, which are R2 technology Inc, intelligent system software Inc. (ISSI), CADx medical systems, and iCAD. All of these commercial CAD systems perform better at detecting calcifications than the masses. Architectural distortions become the challenging task to all the commercial CAD system. One cannot make a direct comparison between these systems and their work because there is no same clinical dataset to study and compare the performances. The proposed CAD model is more suitable for mass detection and classification. The obtained result show that selection of suitable approaches to design an algorithm for CAD is subject to the accuracy, sensitivity, and false positive identifications. To remove background noise and pectoral muscle, region growing and thresholding methods are proved to be good. The quality of the mammography was enhanced by using CLAHE and Wiener. Mass in mammography is extracted with proper marking use of contour-based segmentation. The set relevant features are provided to SVM classifier to discriminate mass type as benign or malignant. Finally, the outcomes from this study predict that the selection of appropriate technique at each stage of medical image analysis is subjective to relevant and significant to design a CAD model.

Author details

Bhagirathi Halalli and Aziz Makandar*

*Address all correspondence to: azizmakandar@kswu.ac.in

Department of Computer Science, Karnataka State Women's University, Karnataka, India

References

[1] Doi K. Computer-aided diagnosis in medical imaging: Historical review, current status and future potential. Computerized Medical Imaging and Graphics. 2017;**31**(4):198-211

[2] Li Q, Nishikawa RM, editors. Computer-Aided Detection and Diagnosis in Medical Imaging. Taylor & Francis, CRC Press, New York; 2015

[3] Chen C-M, Chen, Yi-Hong Chou, Norio Tagawa, and Younghae Do. Computer-aided detection and diagnosis in medical imaging. Computational and Mathematical Methods in Medicine. vol. 2013, Article ID 790608, 2 pages, 2013. doi:10.1155/2013/790608

[4] Giger ML, et al. Computer-aided diagnosis in mammography. Handbook of Medical Imaging. 2nd ed. SPIE Digital Library, Europe, 2000. 915-1004

[5] National Cancer Institutes. Available from: https://www.cancer.gov/types/breast [Accessed: February 10, 2017]

[6] Breast Cancer Organization. Available from: http://www.breastcancer.org/research-news/20130425-4 [Accessed: February 10, 2017]

[7] Debra M. Ikeda. St. Louis, MO: Mosby, Breast Imaging: The Requisites, 2nd ed. 2011, 448 p

[8] Gilbert FJ, Astley SM, Gillan MG, Agbaje OF, Wallis MG, James J, Boggis CR, Duffy SW. Single reading with computer-aided detection for screening mammography. The New England Journal of Medicine. 2008;**359**:1675-1684. DOI: 10.1056/NEJMoa0803545. PMID 18832239

[9] Skaane P, et al. Effect of computer-aided detection on independent double reading of paired screen-film and full-field digital screening mammograms. American Journal of Roentgenology. 2007;**188**(2):377–384

[10] Taylor P, Champness J, Given-Wilson R, Johnston K, Potts H. Impact of computer-aided detection prompts on the sensitivity and specificity of screening mammography. Health Technol Assess. 2005;**9**(6)

[11] Fenton JJ, et al. Influence of computer-aided detection on performance of screening mammography. New England Journal of Medicine. 2017;**356**(14):1399-1409

[12] Mammographic Image Database. Available from: http://www.mammoimage.org/databases/ [Accessed: February 10, 2017]

[13] Suckling J, et al. The mammographic image analysis society digital mammogram database exerpta medica. International Congress Series. 1994;**1069**:375-378

[14] Bird RE, Wallace TW, Yankaskas BC. Analysis of cancers missed at screening mammography. Radiology. 1992;**184**:613-617. DOI: 10.1148/radiology.184.3.1509041

[15] Baker JA, Rosen EL, Lo JY, et al. Computer-aided detection (CAD) in screening mammography: Sensitivity of commercial CAD systems for detecting architectural distortion. American Journal of Roentgenology. 2003;**181**:1083-1088

[16] McLoughlin KJ, Bones PJ, Karssemeijer N. Noise equalization for detection of microcalcification clusters in direct digital mammogram images. IEEE Transactions on Medical Imaging. 2004;**23**(3):313-320

[17] Talha M, Sulong GB, Jaffar A. Preprocessing digital breast mammograms using adaptive weighted frost filter. Biomedical Research. 2016;**27**(4):1407-1412

[18] Ponraj DN, et al. A survey on the preprocessing techniques of mammogram for the detection of breast cancer. Journal of Emerging Trends in Computing and Information Sciences. 2011;**2**(12):656-664

[19] Makandar A, Halalli B. Pre-processing of mammography image for early detection of breast cancer. International Journal of Computer Applications (IJCA). 2016;**144**(3):11-15. ISSN: 0975-8887

[20] Ramani R, Suthanthira Vanitha N, Valarmathy S. The pre-processing techniques for breast cancer detection in mammography images. International Journal of Image, Graphics and Signal Processing. 2013;**5**(5):47

[21] Mustra M, Grgic M, Rangayyan RM. Review of recent advances in segmentation of the breast boundary and the pectoral muscle in mammograms. Medical & Biological Engineering & Computing. 2016;**54**(7):1003-1024

[22] Makandar A, Halalli B. Breast cancer image enhancement using median filter and clahe. International Journal of Scientific & Engineering Research (IJSER). 2015;**6**(4):462-465

[23] Al-Najdawi N, Biltawi M, Tedmori S. Mammogram image visual enhancement, mass segmentation and classification. Applied Soft Computing. 2015;**35**:175-185

[24] Dhungel N, Carneiro G, Bradley AP. Deep learning and structured prediction for the segmentation of mass in mammograms. In: International Conference on Medical Image Computing and Computer-Assisted Intervention. Springer International Publishing; 2015

[25] Cheng HD, et al. Approaches for automated detection and classification of masses in mammograms. Pattern Recognition. 2006;**39**(4):646-668

[26] Cascio DO, Fauci F, Magro R, Raso G, Bellotti R, De Carlo F, Tangaro S, De Nunzio G, Quarta M, Forni G, Lauria A. Mammogram segmentation by contour searching and mass lesions classification with neural network. IEEE Transactions on Nuclear Science. 2006;**53**(5): 2827-2833

[27] Hassan SA, Sayed MS, Farag F. Segmentation of breast cancer lesion in digitized mammogram images. Biomedical Engineering Conference (CIBEC); 11-13 December 2014; Cairo International, Giza, Egypt. IEEE; 2014

[28] Anitha J, Dinesh Peter J, Immanuel Alex Pandian S. A dual stage adaptive thresholding (DuSAT) for automatic mass detection in mammograms. Computer Methods and Programs in Biomedicine. 2017;**138**:93-104

[29] Makandar A, Halalli B. Threshold based segmentation technique for mass detection in mammography. Journal of Computer. 2016;**11**(6):472-478. ISSN: 1796-203x. IF: 0.42

[30] Digabel H, Lantuejoul C. Iterative algorithms. In Actes du Second Symposium European d'Analyse Quantitative des Microstructures en Sciences des Mat_eriaux, Biologie et M_edecine; Caen, 4-7 October 1977; (1978), J.-L. Chermant, Ed., Riederer Verlag, Stuttgart, pp. 85–99.

[31] Lantuejoul C. La squelettisation et son application aux mesures topologiques des mosaques polycristallines [thesis]. Paris: Ecole des Mines; 1978

[32] Sonka M, Hlavac V, Boyle R. Image processing, analysis, and machine vision. Cengage Learning. 2014

[33] Gonzalez RC, Woods RE. Image processing. Digital Image Processing. Pearson edition, South Asia, 2007;**2**:627-676

[34] Makandar A, Halalli B. Combined segmentation technique for suspicious mass detection in mammography. In: IEEE Explore, 2015 International Conference on Trends in Automation, Communications and Computing Technology (I-TACT-15) (Volume: 01); 21-22 Dec. 2015; Bangalore, India. IEEE; 2015. pp. 1-5. DOI: 10.1109/ITACT.2015.7492680

[35] Hao Y-M, Zhu F. Fast algorithm for two-dimensional otsu adaptive threshold algorithm. Journal of Image and Graphics. 2005;**4**:014

[36] Bovis K, Singh S. Detection of masses in mammograms using texture features. In: Proceedings 15th International Conference on Pattern Recognition, 2000; 3–7 Sept. 2000; Barcelona, Spain, Spain. Vol. 2. IEEE; 2000

[37] Truong QD, et al. Feature Extraction and Support Vector Machine Based Classification for False Positive Reduction in Mammographic Images. Frontier and Future Development of Information Technology in Medicine and Education. Netherlands: Springer; 2014. pp. 921-929

[38] Dheeba J, Albert Singh N, Tamil Selvi S. Computer-aided detection of breast cancer on mammograms: A swarm intelligence optimized wavelet neural network approach. Journal of Biomedical Informatics. 2014;**49**:45-52

[39] Wajid SK, Hussain A. Local energy-based shape histogram feature extraction technique for breast cancer diagnosis. Expert Systems with Applications. 2015;**42**(20):6990-6999

[40] Beura S, Majhi B, Dash R. Mammogram classification using two dimensional discrete wavelet transform and gray-level co-occurrence matrix for detection of breast cancer. Neurocomputing. 2015;**154**:1-14

[41] Görgel P, Sertbas A, Uçan ON. Computer-aided classification of breast masses in mammogram images based on spherical wavelet transform and support vector machines. Expert Systems. 2015;**32**(1):155-164

[42] Harikumar R. Performance analysis of neural networks for classification of medical images with wavelets as a feature extractor. International Journal of Imaging Systems and Technology. 2015;**25**(1):33-40

[43] Haralick RM, Shanmugam K, Dinstein I. Textural feartures for image classification. IEEE Transactions on Systems Man and Cybernetics. 1973;**SMC3**(6):610-621

[44] Soh L-K, Tsatsoulis C. Texture analysis of SAR sea ice imagery using gray level co-occurrence matrices. IEEE Transactions on Geoscience and Remote Sensing. 1999;**37**(2): 780-795

[45] Clausi DA. An analysis of co-occurrence texture statistics as a function of grey level quantization. Canadian Journal of Remote Sensing. 2002;**28**(1):45-62

[46] Costa AF, Humpire-Mamani G, Traina AJM. An efficient algorithm for fractal analysis of textures. In: 2012 25th SIBGRAPI Conference on Graphics, Patterns and Images; August 22–25 2012. IEEE; 2012. pp. 39-46

[47] Gorgel P, SERTBAŞ A, Kilic N, Osman O. Mammographic mass classification using wavelet based support vector machine. IU-Journal of Electrical & Electronics Engineering 2009;**9**(1):867-75

[48] Tzikopoulos SD, Mavroforakis ME, Georgiou HV, Dimitropoulos N, Theodoridis S. A fully automated scheme for mammographic segmentation and classification based on breast density and asymmetry. computer methods and programs in biomedicine. 2011;**102**(1):47-63

[49] Liasis G, Pattichis C, Petroudi S. Combination of different texture features for mammographic breast density classification. InBioinformatics & Bioengineering (BIBE), 2012 IEEE 12th International Conference on 2012. 732-737

[50] Muštra M, Grgić M, Delač K. Breast density classification using multiple feature selection. automatika. 2012;**53**(4):362-72

[51] Subashini TS, Ramalingam V, Palanivel S. Automated assessment of breast tissue density in digital mammograms. Computer Vision and Image Understanding. 2010;**114**(1):33-43

Chapter 6

Breast Ultrasound Tomography

Nebojsa Duric and Peter Littrup

Additional information is available at the end of the chapter

http://dx.doi.org/10.5772/intechopen.69794

Abstract

Both mammography and standard ultrasound (US) rely upon subjective criteria within the breast imaging reporting and data system (BI-RADS) to provide more uniform interpretation outcomes, as well as differentiation and risk stratification of associated abnormalities. In addition, the technical performance and professional interpretation of both tests suffer from machine and operator dependence. We have been developing a new technique for breast imaging that is based on ultrasound tomography which quantifies tissue characteristics while also producing 3-D images of breast anatomy. Results are presented from clinical studies that utilize this method. In the first phase of the study, ultrasound tomography (UST) images were compared to multi-modal imaging to determine the appearance of lesions and breast parenchyma. In the second phase, correlative comparisons with MR breast imaging were used to establish basic operational capabilities of the UST system. The third phase of the study focused on lesion characterization. Region of interest (ROI) analysis was used to characterize masses. Our study demonstrated a high degree of correlation of breast tissue structures relative to fat subtracted contrast-enhanced MRI and the ability to scan ~90% of the volume of the breast at a resolution of 0.7 mm in the coronal plane.

Keywords: breast, ultrasound, 3-D imaging, tomography, cancer

1. Introduction

Breast cancer is the most common cancer among women, accounting for one-third of cancers diagnosed. Statistically, ~230,000 new cases of invasive breast cancer and ~63,000 in situ breast carcinomas are diagnosed in the US annually; breast cancer is the third leading cause of cancer death among women, causing ~40,000 deaths in the US every year [1]. According to SEER statistics, approximately 61% of women are found to have localized breast cancers at the time of diagnosis; about 31% are found to be regional disease; another 5% are diagnosed with distant metastases while about 3% are unstaged [2]. The 5-year survival rate for women with localized

cancer is 98%; for those with regional disease, it drops to 84%; for those diagnosed with distant stage, the survival rate drops dramatically to 23%; while for unstaged cancers the 5-year survival rate is about 58%. **Figure 1** illustrates the dependence of survival on cancer stage.

There are many reasons why cancers are not detected early but some of the major factors relate to limited participation in breast screening and the performance of screening mammography.

1.1. Limited participation in screening

National cancer screening statistics indicate that only 51% of eligible women undergo annual mammograms [4]. That rate is even lower for African American women and/or those of lower socioeconomic groups. Access, fear of radiation and discomfort are some of the factors that contribute to the low participation rate. Greater participation would lead to detection of breast cancer at an earlier stage leading to longer survival. Increased participation and improved breast cancer detection would have the greatest effect on the statistic of nearly 1 in 3 women who are diagnosed each year with later stage (regional or greater) breast cancer, totaling approximately 60,000 women per year in the USA. The net effect would be an increase in survival time and a corresponding decrease in mortality rates. This is also suggested in a recent meta-analysis, whereby increased participation and sensitivity lead to additional invasive cancer detection and greater mortality reduction [4].

1.2. Limited performance of mammography

For women with dense breast tissue, who are at the highest risk for developing breast cancer [5–8], the performance of mammography is at its worst [9]. Consequently, many cancers are

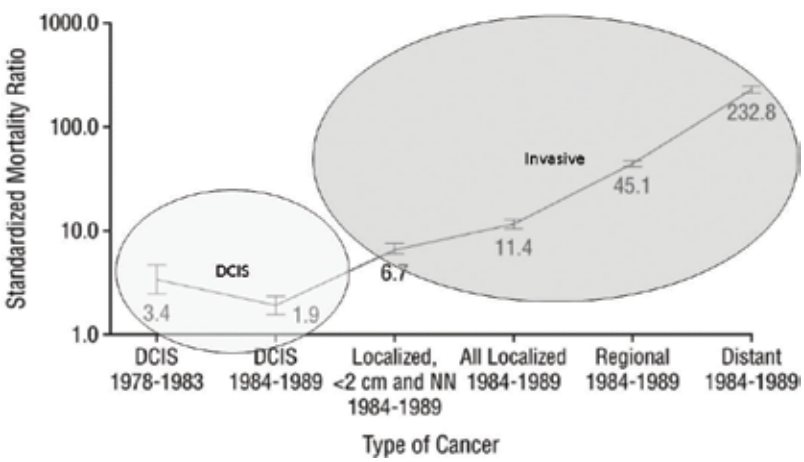

Figure 1. The dependence of mortality rates on cancer type and stage. From Kerlikowske et al. [3].

missed at their earliest stages when they are the most treatable. Improved cancer detection for women with denser breasts would decrease the proportion of breast cancers diagnosed at later stages, which would significantly lower the mortality rate.

1.3. The breast screening challenge

X-ray mammography detects about 5 cancers per 1000 screens [10]. However, its positive predictive value (PPV) is low and its sensitivity is greatly reduced in women with dense breast tissue [10]. Although digital breast tomosynthesis (DBT) may improve upon some of the limitations of standard mammography, it is unlikely to create a paradigm shift in performance [11] while generating even higher levels of ionizing radiation [12]. MRI can significantly improve on these limitations by virtue of its volumetric, radiation-free imaging capability. Studies have shown that MRI can have a positive impact in the breast management continuum ranging from risk assessment to diagnosis and treatment monitoring [12, 13]. However, MRI can have a high false positive rate, requires contrast injection and the exams can be both long and costly [14]. Furthermore, MR has long been prohibitively expensive for routine use and there is a need for a low-cost equivalent alternative. Yet, for high-risk women, MRI is now viewed as the gold standard for breast cancer detection and screening [15–23]. Positron emission tomography is also limited by cost and radiation concerns.

Recent studies have demonstrated the effectiveness of hand held ultrasound imaging in detecting breast cancer, particularly for women with dense breasts (**Table 1**). These studies have shown that up to 4.5 extra cancers were detected per 1000 screens [24–34]. A striking aspect of the added detections is that they are predominantly node negative invasive cancers which would have potentially progressed to a later stage before possible mammographic detection. Moreover, there is little risk of over detection of ductal carcinoma in situ (DCIS). The sensitivity of mammography is greater for DCIS than it is for invasive cancer, with DCIS making up approximately 25% of mammographic screen-detected breast cancers [35].

We have examined the data from these studies to extract the statistics of cancer detection by imaging mode (**Table 1**). The results are summarized in **Figure 2**. It is striking to note that ultrasound (US) almost doubles the cancer detection rate in dense breasts. However, despite these successful study outcomes, handheld ultrasound is unlikely to be adopted for screening because it is operator dependent, and its imaging aperture is small, which hinders whole breast imaging. Furthermore, ultrasound's increased sensitivity to invasive cancer is offset by lowered sensitivity to DCIS by virtue of mammography's greater ability to detect microcalcifications. Although such a trade-off may be justified by the fact that mortality from invasive cancers is much higher than that from DCIS, a combined screening [mammography plus automated breast ultrasound (ABUS)] would provide a comprehensive screen. It has therefore been proposed that ABUS be used for screening, supplemental to mammography.

Author (Year)	Center	Type	Exams	US only cancers	Yield per 1000
Brem et al. (2014)	Multi	ABUS	15,318	30	1.96
Berg et al. (2012)	Multi	HHUS	7473	32	4.28
Hooley et al. (2012)	Single	HHUS	935	3	3.21
Kelly et al. (2010)	Multi	AWBU	6425	23	3.58
Corsetti et al. (2008)	Multi	HHUS	9157	37	4.04
Crystal et al. (2003)	Single	HHUS	1517	7	4.61
Leconte et al. (2003)	Single	HHUS	4236	16	3.78
Kolb et al. (2002)	Single	HHUS	13,547	37	2.73
Kaplan (2001)	Single	HHUS	1862	6	3.22
Buchberger et al. (2000)	Single	HHUS	8103	32	3.95
Gordon et al. (1995)	Single	HHUS	12,706	44	3.46

Table 1. Summary of studies used in the analysis.

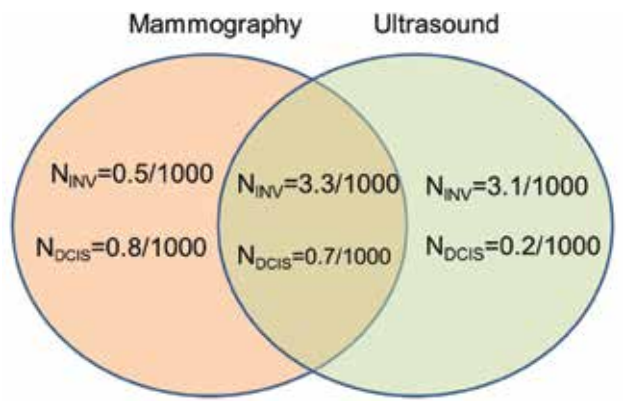

Figure 2. Venn diagram summarizing comparative cancer detection rates for screening mammography and ultrasound.

To that end, automated breast ultrasound (ABUS) has been introduced as a way of overcoming these issues, mainly by reducing operator dependence and increasing the field of view. For example, the GE Invenia ABUS ultrasound system for breast cancer screening, originally developed by U-Systems., recently received screening approval, adjunctive to mammography, from the FDA, because it demonstrated an ability to detect cancers missed by mammography in dense breasts. The SomoInsight screening study [24], indeed showed that ABUS plus mammography outperformed mammography alone, leading to the first FDA approval for ultrasound screening for breast cancer.

The fundamental quandary of breast screening today is the knowledge that (i) mammography misses cancers in dense breasts, (ii) that Automated Breast ultrasound (ABUS) detects cancers that mammography misses and yet (iii) screening continues largely with mammography only. This paradox

is amplified even further by the proliferation of state breast density notification laws in the USA which mandate that this information be available to women undergoing breast cancer screening. The primary reason this paradox exists today is that ABUS screening increases call back rates (up to a factor of two in case of the SomoInsight study [23]). The improvement in classification performance, measured by the area under the ROC curve, is modest because the increase in sensitivity is partially offset by an increase in false positives thus slowing its adoption. Technically, with its basic B-mode capability, ABUS has the same issue with false positives as hand held ultrasound. It is therefore unlikely that ABUS will be widely adopted for screening in the foreseeable future without more tissue-specific imaging capability. Improved lesion characterization would help lower the barriers to adoption of screening ultrasound.

1.4. Potential role of UST

Ultrasound tomography (UST) is an emerging technique that has the potential for tissue-specific imaging and characterization, by virtue of its transmission imaging capability [36–61]. Improved specificity would lower call back rates and lower the barriers to adoption. An adjunctive use of UST would have the potential to improve specificity relative to current ABUS and provide a comprehensive screen that would uncover invasive cancers otherwise missed by mammography. Detection of such early stage invasive cancers would provide women with curative treatment, the opportunity for which might be otherwise lost.

Conventional reflection ultrasound exploits differences in acoustic impedance between tissue types to provide anatomical images of breast tumors [62, 63]. However, reflection is just one aspect of a multi-faceted set of acoustic signatures associated with the biomechanical properties of tissue. UST is a technique that moves beyond B-mode imaging by virtue of its transmission capabilities. The latter provides additional characterization by measuring tissue parameters such as sound speed and attenuation (ATT) [64–68]. These parameters can be used to characterize lesions in a quantitative manner, a capability not available in current whole breast ultrasound systems. By merging reflection images with images of the bio-acoustic parameters of sound speed and attenuation, UST offers the possibility of exploiting differences in anatomical and physical properties of tissue to accurately differentiate cancer from normal tissue or benign disease. UST parameters are also quantitative, which allows new consideration of second and third-order statistical image analyses, or radiomics. Ultrasound has previously not been suitable for the burgeoning applications of radiomics due to its lack of true quantitative parameters such as sound speed (m/s) and attenuation (dB/cm/MHz). Initial assessments of UST performance was carried out, as described below.

In an initial attempt to assess the potential of UST in breast imaging, studies were carried out at the Karmanos Cancer Institute, Detroit, MI, USA. Informed consent was obtained from all patients, prospectively recruited in an IRB-approved protocol following HIPAA guidelines. Patients were scanned at the Alexander J Walt Comprehensive Breast Center. Standard multi-modality imaging was available for all patients. The Walt Breast Center houses SoftVue, a UST system manufactured by Delphinus Medical Technologies, Inc (Novi, MI). SoftVue embodies a number of attributes that differentiate it from conventional imaging modalities:

- *Water-based pulse coupling*: SoftVue utilizes a water filled imaging chamber that is kept at body temperature. Its primary purpose is to couple the sound energy between the transducer and the breast tissue.
- *Closed geometry probe*: A circular ring transducer surrounds the breast while both are immersed in water. There is no compression of the breast since the transducer is offset from the breast with water acting as the pulse coupling agent. The closed transducer geometry allows collection of signals that pass through the entire width of the breast, a requirement for transmission imaging and the reconstruction of sound speed and attenuation images. These parameters provide quantitative information in absolute units that are tied to externals standards (km/s and dB/cm, respectively).
- *Operator independence*: Unlike mammography and other ABUS systems, multiple positionings are not required for larger breasts. Once the patient is positioned on the table, the operator simply presses the button and the exam is performed automatically without further intervention from the operator.
- *Scan time*: SoftVue scan time is 1–2 min per breast (depending on breast size). This scan duration minimizes intra-slice and inter-slice motion artifacts.
- *Image reconstruction time*. In this study, reconstruction time for a bilateral breast exam was ~30 min for the average patient and current hardware/software processing ability.

SoftVue was used to scan the recruited patients for this study. Coronal image series were produced by tomographic algorithms for reflection, sound speed and attenuation. All images were reviewed by a board-certified radiologist who has more than 20 years of experience in breast imaging and US-technology development. Symptomatic study participants were scanned with a SoftVue UST system. Pathological correlation was based on biopsy results and standard imaging (e.g. US definitive cyst).

Tomographic algorithms were used to generate images stacks of reflectivity, sound speed and attenuation for each patient. Lesions were identified based on correlation with standard imaging so that the tumor sound speed (SS) and attenuation (ATT) could be assessed. An example each type of image is shown in **Figure 3**.

In the first phase of the study, correlative comparisons with multi-modal imaging were carried out to assess lesion properties relative to mammography, US and MR. In the second

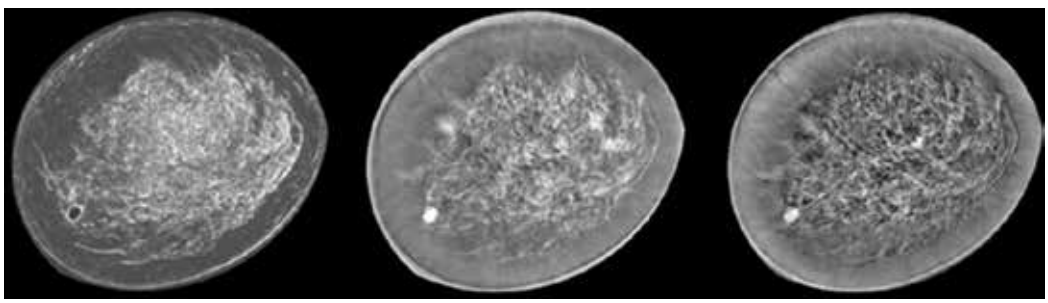

Figure 3. From left to right, reflection, sound speed and attenuation image slices depicting breast parenchyma and a fibroadenoma at 7 o'clock.

http://dx.doi.org/10.5772/intechopen.69794

phase, MR breast imaging was used to establish basic operational capabilities of the UST system including the identification and characterization of parenchymal patterns, determination of the spatial resolution of UST and an estimate the breast volume that can imaged with UST. The third phase of the study focused on lesion characterization. Region of interest (ROI) analyses were performed on all identified lesions using all three UST image types. Combinations of the ROI generated quantitative values were used to characterize all masses, particularly in relation to relative differences with surrounding peritumoral regions.

2. Multi-modal comparisons

Since the patients were recruited at KCI on the basis of having a suspicious finding, standard imaging such as mammography, US and sometimes MRI were available, as well as the radiology and pathology reports. These images and the associated reports were used to retroactively locate the lesions in the UST image stacks for visual comparison. **Figures 4–7** show examples of UST images in relation to the other modalities. When MRI was available, the images were projected into the coronal plane for easier comparison with the UST whose native format is coronal.

Figure 4 shows a 9mm IDC at 3 o'clock. CC and MLO mammographic views of the affected breast are shown on the left with the lesion identified by arrows. The UST views corresponding

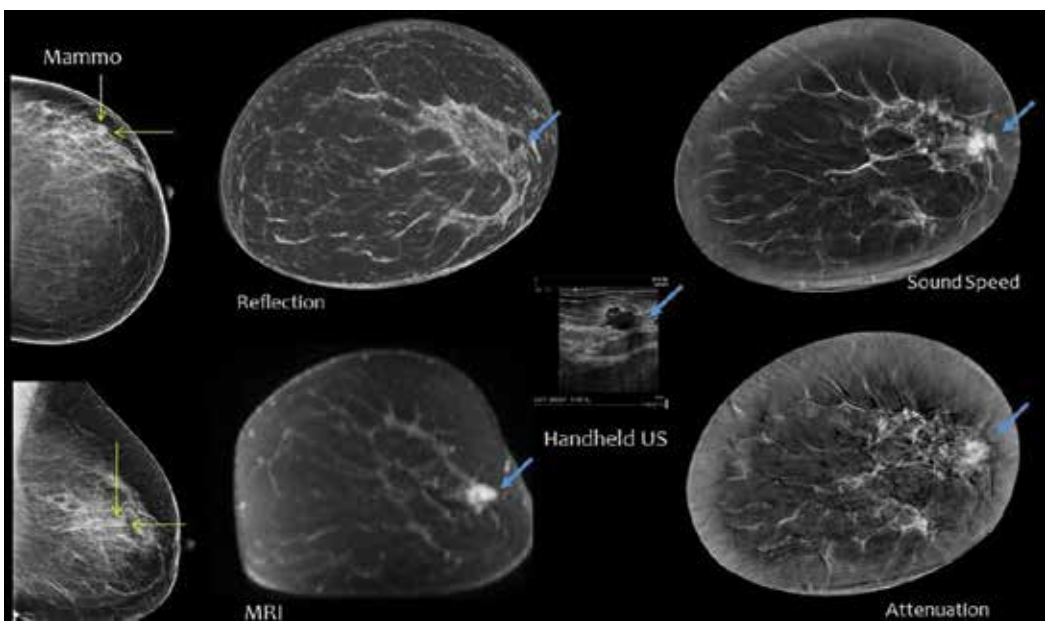

Figure 4. A 9 mm IDC at 3 o'clock. CC and MLO mammographic views of the affected breast are shown on the left with the lesion identified by arrows. The coronal UST views are shown in the form of reflection, sound speed and attenuation images. The corresponding ultrasound and MR images are also shown.

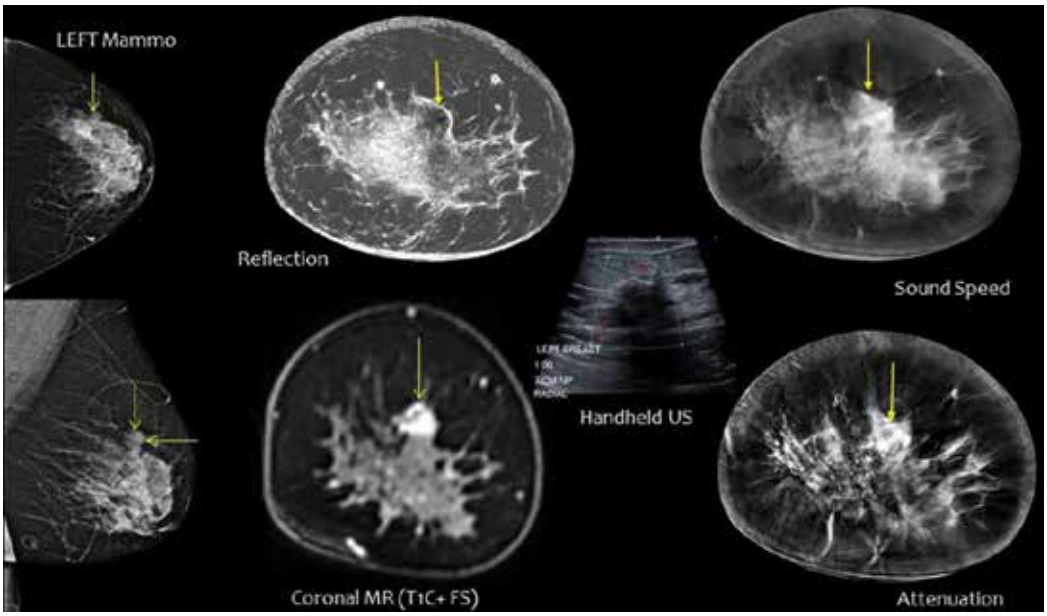

Figure 5. Multimodality images compared to UST reflection, sound speed and attenuation. An IDC is shown at 12 o'clock.

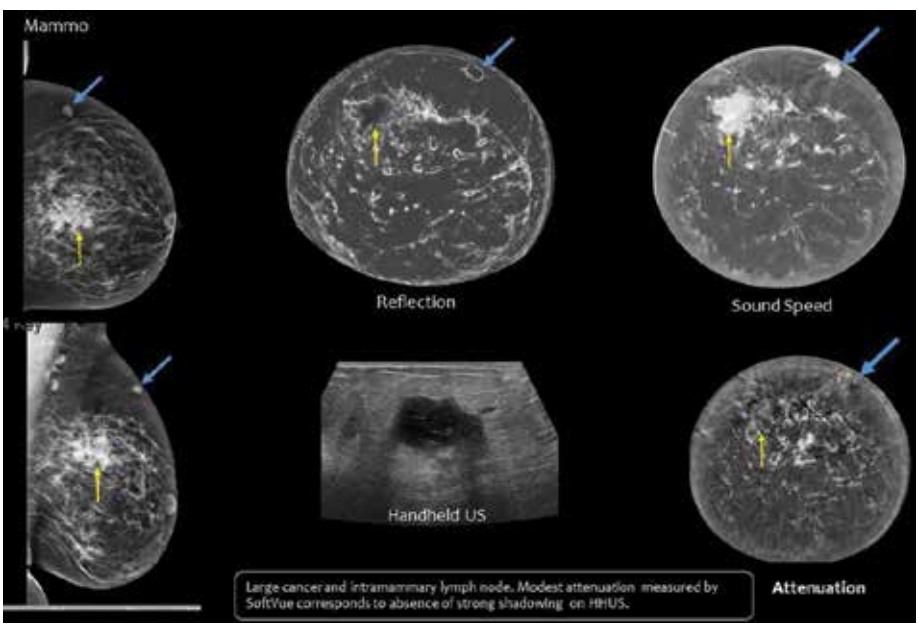

Figure 6. Multimodality images vs UST reflection, sound speed and attenuation showing an IDC and intramammary lymph node.

http://dx.doi.org/10.5772/intechopen.69794

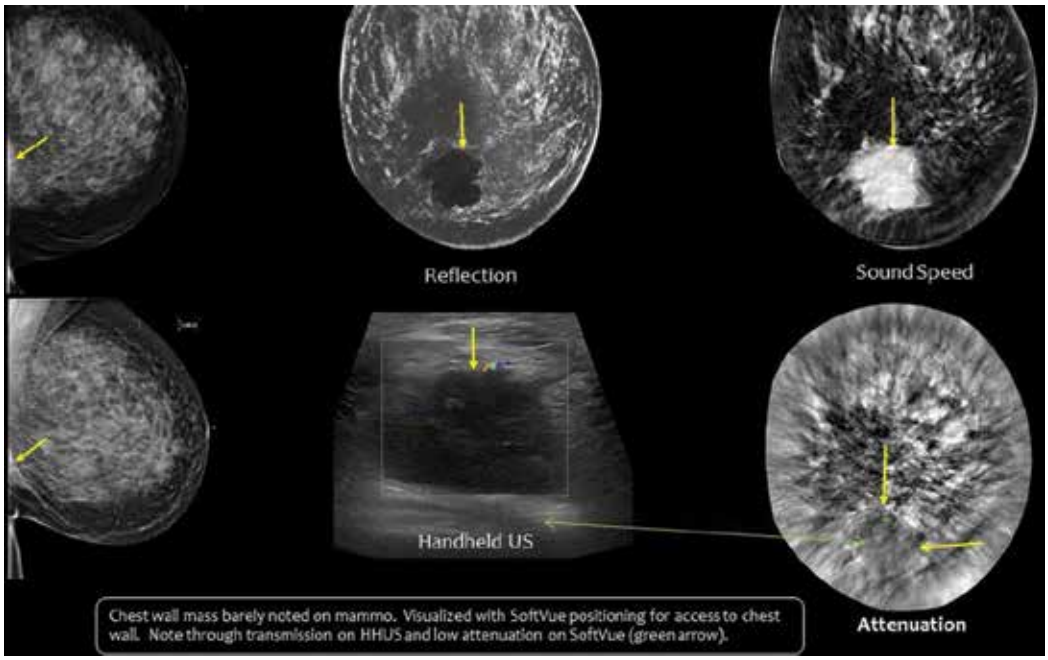

Figure 7. Illustrating the chest wall access achievable by UST relative to mammography.

to the coronal planes that contain the lesions are across the top with reflection, sound speed and attenuation images laid out from left to right. The corresponding ultrasound and MR images are shown along the bottom. Inspection of the images shows good correspondence in shape and location of the lesion. The greatest similarity is between the UST images and MRI. The IDC is seen to be hypoechoic in reflection and has high sound speed and attenuation contrast. An IDC in a heterogeneously dense breast is shown in **Figure 5** This IDC was initially missed by mammography. A large IDC and an intramammary lymph node are shown in **Figure 6**. Note the concordance between the UST images and mammography. **Figure 7** illustrates the chest wall access achievable by UST relative to mammography. Although UST does not access the entire axilla it does visualize the cancer that has invaded the chest wall.

3. MR concordance

UST and MR imaging was performed within weeks of each other. UST imaging was carried out with the SoftVue system (Delphinus Medical Technologies) and the MR exams with a Philips Achieva 3T system. The resulting image sequences were qualitatively and quantitatively to assess imaging performance of UST. As discussed above, UST images correlate best with MR images. Further inspection shows that of the three UST image types, the sound speed image correlates best with MR. **Figure 8** shows a coronal view comparison between UST speed of sound and MR contrast-enhanced fat subtracted images of representative breast parenchyma.